XRCC1 mutation is associated with PARP1 hyperactivation and cerebellar ataxia

Article (Accepted Version)

XRCC1 Mutation is Associated with PARP1 Hyperactivation and Cerebellar Ataxia

Nicolas Hoch[1,2*], Hana Hanzlikova[1*], Stuart L. Rulten[1], Martine Tétreault[3], Emilia Koumulainen[1], Limei Ju[1], Peter Hornyak[1], Zhihong Zeng[1], William Gittens[1], Stephanie Rey[4], Kevin Staras[4], Grazia M.S. Mancini[5], Peter J. McKinnon[6], Zhao-Qi Wang[7], Justin Wagner[8], Care4Rare Canada Consortium, Grace Yoon[9**] and Keith W. Caldecott[1**]

*these authors contributed equally
**Corresponding authors.

1. Genome Damage and Stability Centre, School of Life Sciences, University of Sussex, Falmer, Brighton, UK
2. CAPES Foundation, Ministry of Education of Brazil, Brasilia/DF 70040-020, Brazil
3. Department of Human Genetics, McGill University and Genome Québec Innovation Centre, Montréal, Québec, H3A 0G4, Canada,
4. Neuroscience, School of Life Sciences, University of Sussex, Falmer, Brighton, UK
5. Department of Clinical Genetics, Erasmus MC, P.O. Box 2040, 3000 CA, Rotterdam, the Netherlands
6. St Jude Children's Research Hospital, Memphis, USA
7. Leibniz Institute for Age Research, Fritz Lipmann Institute, 1107745 Jena, Germany
8. The Children's Hospital of Eastern Ontario Research Institute, Ottawa, K1L 8H1, Canada,
9. Division of Clinical and Metabolic Genetics, and Division of Neurology, The Hospital for Sick Children, University of Toronto, Toronto, M5G 1X8, Canada,

Correspondence to: Keith W. Caldecott (k.w.caldecott@sussex.ac.uk) and Grace Yoon (grace.yoon@utoronto.ca)

XRCC1 is a molecular scaffold protein that assembles multi-protein complexes involved in DNA single-strand break repair[1,2]. Here, we show that biallelic mutations in human *XRCC1* are associated with ocular motor apraxia, axonal neuropathy, and progressive cerebellar ataxia. *XRCC1*-mutant patient cells exhibit not only reduced rates of single-strand break repair but also elevated levels of protein ADP-ribosylation; a phenotype recapitulated in a related syndrome caused by mutations in the XRCC1 partner protein PNKP and implicating hyperactivation of poly (ADP-ribose) polymerase/s as a cause of cerebellar ataxia. Indeed, remarkably, genetic deletion of *Parp1* rescued normal cerebellar ADP-ribose levels and reduced the loss of cerebellar neurons and ataxia in *Xrcc1*-defective mice, identifying a molecular mechanism by which endogenous single-strand breaks trigger neuropathology. Collectively, these data establish the importance of XRCC1 protein complexes for normal neurological function and identify PARP1 as a therapeutic target in DNA strand break repair-defective disease.

A forty-seven year old woman of East Indian descent and non-consanguineous parents was diagnosed at age forty-one with cerebellar atrophy, gait and limb ataxia, ocular motor apraxia, and peripheral neuropathy (Fig. 1a, b). Prenatal and early developmental history was completely normal and difficulties with balance and gait were first noticed at twenty-eight years, but this was not fully investigated until age forty. Magnetic resonance imaging (MRI) and cerebellar examination revealed progressive cerebellar atrophy (Fig. 1c) and multiple ataxic abnormalities including dysmetria, dysdiadochokinesis, and dysarthria, and nerve conduction studies revealed chronic length-dependent sensory-motor predominantly axonal peripheral neuropathy (Fig. 1b, Supplementary Information). After ruling out more than ten known spinocerebellar ataxias by genetic and metabolic screening (Supplementary Information) exome sequencing of the proband identified compound heterozygous mutations in *XRCC1* (NM_006297). The mutations were confirmed by Sanger sequencing as c.1293G>C (p.K431N) and c.1393C>T (p.Q465*) and were present *in trans*, with the unaffected sibling of the proband heterozygous for c.1293G>C (Fig. 1d). c.1393C>T has not previously been described in the population, whereas

c.1293G>C was previously detected in heterozygous state in four individuals of South Asian descent (ExAC Consortium, Cambridge, MA). After ruling out other rare gene variants on the basis of their presence in the unaffected sibling, presence in homozygous state in unaffected in-house controls and/or ExAC, and lack of functional and/or disease relevance no other candidate causative mutations remained.

The c.1393C>T mutation is located within exon 12 and creates a premature stop codon at amino acid 465, most likely triggering nonsense mediated mRNA decay. The c.1293G>C mutation is located at the end of exon 11 and is also part of the donor splice site for intron 11, most likely affecting splicing and inducing premature stop codons/nonsense-mediated decay and/or encoding XRCC1 with the missense mutation, K431N. Consistent with this, reduced total levels of XRCC1 mRNA were observed in patient cells, as well as aberrant splicing of XRCC1 transcripts if nonsense-mediated decay was inhibited with cycloheximide (Extended Data Fig. 1).

To establish the pathogenic impact of the biallelic *XRCC1* mutations we examined patient fibroblasts and lymphoblastoid cells (LCLs) for levels of XRCC1 protein by indirect immunofluorescence and Western blotting. The level of XRCC1 in the patient primary fibroblasts was greatly reduced when compared to wild type primary human fibroblasts (1BR) by indirect immunofluorescence and was not measurably higher than in human RPE-1 cells in which *XRCC1* was deleted by CRISPR-Cas9 (Fig. 2a). However, Western blotting suggested that patient fibroblasts and LCLs both retained a small amount (~5%) of residual XRCC1 (Fig. 2b, Extended Data Fig. 2a). Indeed, this was confirmed using XRCC1 siRNA, which reduced the anti-XRCC1 signal on Western blots of patient fibroblasts even further (Fig. 2b, *bottom*). Levels of DNA ligase IIIα (Lig3α) were also greatly reduced (by >80%) in patient cells, consistent with the established impact of XRCC1 on the cellular stability of this partner protein (Fig. 2b, *top*, Extended Data Fig. 2b)[3-5]. Since germ-line deletion of *Xrcc1* in mouse is embryonic lethal[6] we suggest that the small amount of XRCC1 remaining in the patient was important for embryonic viability. Consistent with this idea, embryonic viability in mice is supported by a little as ~10% of normal Xrcc1 levels[7].

To determine whether the residual XRCC1 in patient cells can engage in single-strand break repair (SSBR) we quantified the extent to which it bound oxidised chromatin. XRCC1 was primarily detected in nucleoli in undamaged wild-type RPE-1 cells and normal primary 1BR fibroblasts, following the extraction of soluble proteins with detergent, but was rapidly recruited into global nuclear chromatin following treatment with H_2O_2 (Fig. 2c, d); a physiological source of oxidative single-strand breaks (SSBs)[8]. In contrast, little or no XRCC1 recruitment into chromatin was detected in *XRCC1*-patient fibroblasts by high-resolution or high-content imaging (Fig. 2c, d, Extended Data Fig. 3a). Similar results were observed following treatment with camptothecin (CPT), a topoisomerase poison that induces SSBs triggered by abortive topoisomerase I activity (Extended Data Fig. 3b).

Importantly, the defect in XRCC1 recruitment in patient fibroblasts was accompanied by a delay in the kinetics of DNA single-strand break repair (SSBR) following H_2O_2 treatment (Fig. 3a). This phenotype was recapitulated in *XRCC1*$^{-/-}$ RPE-1 cells and is consistent with the established molecular role of XRCC1[2,9]. In contrast, we failed to detect a major difference in double-strand break repair in *XRCC1*-patient fibroblasts, as measured by γH2AX immunostaining following ionising radiation (Fig. 3b, Extended Data Fig. 4). In agreement with the defect in SSBR, *XRCC1*-patient LCLs exhibited a four-fold increase in sister chromatid exchange; a hyper-recombination phenotype resulting from elevated homologous recombination triggered by unrepaired SSBs in S/G2 phase of the cell cycle (Fig. 3c)[10,11].

XRCC1 is a scaffold protein that assembles SSBR multi-protein complexes and, importantly, components of these complexes are mutated in the cerebellar ataxias *spinocerebellar ataxia with axonal neuropathy-1* (SCAN1; mutated in TDP1)[12,13], *ataxia oculomotor apraxia-1* (AOA1; mutated in Aprataxin)[14], and *ataxia oculomotor apraxia-4* (AOA4; mutated in PNKP)[15,16]. Indeed, it is striking that the pathology of the XRCC1 patient combines features of each of these diseases, consistent with the role played by XRCC1 in coordinating their activity. The discovery that XRCC1 is itself mutated in cerebellar ataxia is thus significant because it demonstrates the importance of these complexes in preventing neurodegeneration in humans.

To investigate the mechanism(s) by which unrepaired SSBs trigger neuropathology we considered the possibility that persistent unrepaired SSBs might result in prolonged activity of the SSB sensor protein, PARP1. This hypothesis was prompted by the observation that excessive synthesis of poly (ADP-ribose) and/or excessive depletion of NAD^+ by PARP1 is neurotoxic and associated with ischemia reperfusion injury[17,18]. Consistent with this idea, whilst ADP-ribose was rapidly detected in both wild type and patient fibroblasts following H_2O_2 treatment it persisted at a higher level in the latter cells during subsequent incubation in drug-free medium (Fig. 4a, *left*). This was also evident in *XRCC1*$^{-/-}$ human RPE-1 cells, confirming that this phenotype was induced by loss of XRCC1. Elevated ADP-ribose levels were also detected in XRCC1 patient fibroblasts and *XRCC1*$^{-/-}$ RPE-1 cells following treatment with camptothecin (CPT) (Fig. 4a, *right*). Indeed, the difference in ADP-ribose levels between wild type and XRCC1-mutant cells was even greater following CPT than following H_2O_2 treatment. The type of SSB induced by CPT has been linked previously with SSBR-defective neurodegenerative disease and is a possible source of pathogenic SSBs in SSBR-defective individuals[13,19]. Consistent with this idea, CPT-induced ADP-ribose levels were also elevated in fibroblasts from a patient with ataxia oculomotor apraxia-4 (AOA4); the cerebellar ataxia resulting from mutation of the XRCC1 protein partner, PNKP (Fig. 4b, Extended Data Fig. 5). Importantly, the elevated ADP-ribose observed in CPT-treated *XRCC1*$^{-/-}$ RPE-1 cells, *XRCC1*- patient cells, and PNKP-patient cells was entirely dependent on PARP1 activity (Fig. 4c, Extended Data Figs 6, 7). Moreover, this phenotype was rescued by the introduction of wild-type recombinant XRCC1 into XRCC1 patient fibroblasts by electroporation (Fig. 4d, Extended Data Fig. 8).

Next, to examine directly whether hyperactive PARP1 triggers cerebellar ataxia in the absence of efficient SSBR we employed a mouse model in which *Xrcc1* was conditionally deleted in brain (*Xrcc1*$^{Nes\text{-}Cre}$)[4]. *Xrcc1*$^{Nes\text{-}Cre}$ mice exhibit pronounced cerebellar histopathology including increased apoptosis of cerebellar granule neurons[4], greatly reduced numbers of cerebellar interneurons[4], and decreased electrophysiological spike activity in Purkinje cells (Extended Data Fig. 9). Moreover, consistent with the pathology of the *XRCC1*-mutant patient and other SSBR-defective patients, *Xrcc1*$^{Nes\text{-}Cre}$ mice exhibit cerebellar ataxia[4]. Strikingly, we detected elevated levels of ADP-ribose in the cerebellum of

Xrcc1$^{Nes\text{-}Cre}$ mice suggesting that the loss of Xrcc1 can trigger Parp1 hyper-activation in brain even at endogenous levels of SSBs (Fig. 4e). Indeed, the deletion of *Parp1* ablated both the elevated level of ADP-ribose and the characteristic loss of cerebellar interneurons in *Xrcc1*$^{Nes\text{-}Cre}$ mice, thereby increasing neuronal density in the molecular layer ~4-fold to wild type levels (Fig. 5a, b). This did not reflect an impact of Parp1 deletion on the rate of SSBR because the latter was similarly slow in *XRCC1*$^{-/-}$ and *XRCC1*$^{-/-}$/*PARP1*$^{-/-}$ RPE-1 cells (Extended Data Fig. 10). Rather, these data demonstrate that in the absence of Xrcc1-dependent SSB repair Parp1 is hyperactivated, resulting in the loss and/or dysfunction of cerebellar neurones. Finally, to examine whether *Parp1* deletion also rescued the cerebellar ataxia observed in *Xrcc1*$^{Nes\text{-}Cre}$ mice we compared *Xrcc1*$^{Nes\text{-}Cre}$ and *Xrcc1*$^{Nes\text{-}Cre}$/*Parp1*$^{-/-}$ mice for their performance on an accelerating rotarod. Indeed, remarkably, whereas *Xrcc1*$^{Nes\text{-}Cre}$ mice were profoundly ataxic and unable to remain on the rotarod for more than a few seconds the additional deletion of *Parp1* improved the rotarod performance of *Xrcc1*$^{Nes\text{-}Cre}$ mice >30-fold, increasing their mean retention time to ~30 sec (Fig. 5c).

Collectively, these data identify elevated ADP-ribose levels as a biomarker of PARP1 hyperactivity and as a cause of cerebellar ataxia induced by unrepaired SSBs (Fig. 5d). This scenario might also extend to other more common neurodegenerative diseases because elevated levels of oxidative stress and DNA strand breakage are also implicated in diseases such as Alzheimer's disease, Huntington's disease, and Parkinson's disease[20-22]. Finally, these data identify PARP1 as a possible drug-target for the treatment of cerebellar ataxias associated with unrepaired SSBs. Inhibition of PARP1 with currently available chemical inhibitors may not be useful in this context, however, because these inhibitors "trap" PARP1 on DNA[23] and do not mimic PARP1 genetic deletion (Extended Data Fig. 10). However, the development of selective inhibitors of PARP1 that prevent DNA binding by this enzyme may have significant therapeutic potential.

Figure Legends

Figure 1. Biallelic XRCC1 mutations are associated with cerebellar ataxia, ocular motor apraxia and axonal neuropathy. ***a***, Family pedigree of the affected proband (III.1; black circle) and her unaffected sister (III.2; circle with black dot). ***b***, Summary of proband clinical features. The full clinical history and electrophysiological analysis is presented in Supplementary Information. ***c***, MRI of the proband at age 40 and 47. Sagittal T1 weighted images (*middle top*) demonstrating moderately severe vermian atrophy and Axial FLAIR images (*right top*) demonstrating atrophy of the cortex of the vermis and cerebellar hemispheres at age 40. Note that imaging at age 47 reveals progression of the vermian atrophy and atrophy of the vermian cortex and cerebellar hemispheres (*bottom*). The cerebellum is circled in white and insets (*left*) are magnifications of the sagittal images to highlight the cerebellar atrophy. ***d***, Confirmation by Sanger sequencing of the mutations c.1293G>C (p.K431N) and c.1393C>T (p.Q465*) in the proband (III.1) and c.1293G>C (p.K431N) in the unaffected sibling (III.2).

Figure 2. XRCC1 patient mutations greatly reduce XRCC1 protein levels and XRCC1 recruitment into damaged chromatin. ***a***, 1BR wild type human fibroblasts ("WT Fib.") and wild type RPE-1 cells ("WT RPE-1") were compared with *XRCC1* patient fibroblasts ("Patient Fib.") and *XRCC1*$^{-/-}$ RPE-1 cells for levels of XRCC1 protein by indirect immunofluorescence. Cells were counterstained with DAPI and images captured on a Zeiss microscope. ***b,*** ***Top***, wild type RPE-1 cells, wild type 1BR fibroblasts, and wild type lymphoblastoid cells ("LCLs") were compared with *XRCC1*$^{-/-}$ RPE-1 cells, *XRCC1* patient fibroblasts, and with LCLs from the XRCC1 patient or the unaffected sibling for levels of XRCC1, Lig3α, and Tubulin by Western blotting. *Bottom,* wild type or patient fibroblasts were transfected with non-targeting or XRCC1 siRNA and XRCC1 and Tubulin protein levels analysed by Western blotting. ***c***, XRCC1 recruitment into chromatin was compared in the indicated cell lines before and 10 min after treatment with 1 mM H_2O_2. Cells were pre-extracted with detergent prior to fixation and immunostaining, and images were captured as above. ***d***, Quantitation of XRCC1 in chromatin (excluding the nucleoli) from >1000 cells per sample using Olympus ScanR acquisition and analysis software. Data are the mean (+/-1SD) of three independent experiments. Statistical significance (two-

tailed t-test) was assessed where indicated (**p<0.01; “ns”, not significant). Representative ScanR images are shown in Extended Data Fig. 3a. Scale bars are 10 μm.

Figure 3. Defective DNA single-strand break repair in *XRCC1*-mutant patient cells. ***a***, DNA strand breakage was quantified by alkaline comet assays in wild type RPE-1 cells, *XRCC1*$^{-/-}$ RPE-1 cells, normal human fibroblasts (1BR), and *XRCC1*-mutated patient fibroblasts before and immediately after treatment with H_2O_2 on ice and after the indicated repair periods in drug-free medium. Data are the average comet tail moment (an arbitrary unit-measure of DNA strand breaks) of 100 cells per sample and are the mean (+/-SEM) of three independent experiments. Statistically significant differences (two-way ANOVA) are indicated (*p<0.05; **p<0.01). ***b,*** γH2AX foci were quantified as a measure of DSBs in the indicated cell lines before and at the indicated times after ionising radiation (2 Gy). Data are the average number of γH2AX foci per cell from ~1000 cells/sample and are the mean (+/-1SD) of three independent experiments. Data were quantified by ScanR high content imaging. Statistically significant differences (two-way ANOVA) are indicated (**p<0.01; ns, not significant). Representative images are presented in Extended Data Fig. 4. ***c***, Representative images (*left*) and quantification (*right*) of sister chromatid exchanges in LCLs from an unrelated normal control (“WT”), the unaffected sibling, and the *XRCC1*-mutated patient. A total of 36 metaphases per genotype were scored and the mean number of SCEs (+/-1SEM) per chromosome was plotted for each metaphase. Statistically significant differences (two-tailed t-test) are indicated (**p<0.01; ns, not significant). Scale bars are 10 μm.

Figure 4. Elevated ADP-ribosylation in XRCC1-mutated patient cells and cerebellum. *a*, Levels of ADP-ribosylation were measured in 1BR wild type human fibroblasts (“WT Fib.”), wild type RPE-1 cells (“WT RPE-1”), *XRCC1* patient fibroblasts (“Patient Fib.”), and *XRCC1*$^{-/-}$ RPE-1 cells by indirect immunofluorescence using Anti-pan-ADP-ribose binding reagent (Millipore). Cells were treated with 150 μM H_2O_2 for 10 min and then incubated in drug-free medium for 60 min to allow DNA repair or were incubated with 30 μM CPT for

45 min. ***b***, *Left*, ADP-ribosylation was detected in 1BR wild type and PNKP patient fibroblasts after CPT treatment by indirect immunofluorescence as above. *Middle*, Western blot showing PNKP, XRCC1, and PARP1 levels in the two cell lines. *Right*, Quantitative comparison of ADP-ribose levels in 1BR wild type, XRCC1-mutant patient, and PNKP patient fibroblasts before and after CPT treatment, measured by ScanR imaging and plotted relative to the ADP-ribose level in untreated 1BR cells. Data are from >1000 cells/sample and are the mean (+/-1SD) of three independent experiments. Statistically significant differences (two-tailed t-test) are indicated (*p<0.05). ***c***, ADP-ribosylation was detected in wild type ("WT"), *XRCC1*$^{-/-}$, *PARP1*$^{-/-}$, and *XRCC1*$^{-/-}$/*PARP1*$^{-/-}$ RPE-1 cells after CPT treatment by indirect immunofluorescence as above. ***d,*** Levels of ADP-ribosylation were quantified before and after CPT treatment by high content imaging as above in wild type 1BR fibroblasts, XRCC1 patient fibroblasts ("X1 pat."), and XRCC1 patient fibroblasts transfected by electroporation in the presence of 1 µg or 2 µg, as indicated, of control BSA or purified recombinant human XRCC1-His protein. Statistically significant differences (two-tailed t-test) to CPT treated 1BR cells are indicated (*p<0.05). Representative ScanR images are presented in Extended Data Figure 8. ***e,*** Levels of ADP-ribosylation were measured in cerebellar sections from *wild type* (WT), *Xrcc1*$^{Nes\text{-}Cre}$ (Xrcc1 KO), *Parp1*$^{-/-}$ (Parp1 KO), and *Xrcc1*$^{Nes\text{-}Cre}$/*Parp1*$^{-/-}$ (Xrcc1 KO/Parp1 KO) mice by immunohistochemistry using rabbit anti-poly (ADP-ribose) primary antibody (Trevigen). Scale bars in IF images are 10 µm and in the histology section is 1 mm.

Figure 5. *Parp1* deletion restores normal interneuron density and reduces cerebellar ataxia in *XRCC1*$^{Nes\text{-}Cre}$ mice. ***a***, Neurons in cerebellar sections from *wild type* (WT), *Xrcc1*$^{Nes\text{-}Cre}$ (Xrcc1 KO), *Parp1*$^{-/-}$ (Parp1 KO), and *Xrcc1*$^{Nes\text{-}Cre}$/*Parp1*$^{-/-}$ (Xrcc1 KO/Parp1 KO) mice were detected by Nissl staining. The position of the granule layer ("*gl*"), molecular layer ("*ml*"), and Purkinje cells ("*pc*") is indicated. Note the reduced number of interneurons (black arrows) in the molecular layer of *Xrcc1*$^{Nes\text{-}Cre}$ mice. Representative images are shown and scale bars are 200 µm. ***b***, Quantitation of interneuron density in the molecular layer in mouse cerebellum of the indicated genotype. Data are the mean (+/-SEM) Nissl-positive cells per µm^2 in the molecular layer of sections from 5-10 mice per

genotype. T-test comparisons are indicated (**p<0.01, ***p<0.001). ***c,*** Motor coordination/cerebellar ataxia was measured in mice of the indicated genotype on an accelerating rotarod. The number of mice analysed for each genotype are indicated in/above the bars. Statistically significant t-test comparisons are indicated (**p<0.01, ***p<0.001). ***d***, Model for PARP1 hyperactivation and neural death triggered by unrepaired SSBs. PARP1 binding and activation at SSBs results in ribosylation of itself and histones with poly (ADP-ribose) (red wavy lines). Poly (ADP-ribose) binding by XRCC1 assembles protein complexes containing the enzymes required for repair of the SSBs. However, if SSB repair is inefficient, PARP1 activity persists resulting in excessive poly (ADP-ribose) and concomitant depletion of NAD^+; both of which are implicated in cytotoxicity. Protein partners associated previously with cerebellar ataxia in humans are highlighted in red and their associated cerebellar ataxias are boxed in red. SCAN1; *spinocerebellar ataxia with axonal neuropathy-1* (mutated in *TDP1*). AOA1; *ataxia oculomotor apraxia-1* (mutated in *APTX*). AOA4; *ataxia oculomotor apraxia-4* (mutated in *PNKP*). We suggest that the patient with XRCC1 mutations will be the founder member of a new Syndrome; *ataxia oculomotor apraxia-XRCC1* (*AOA-XRCC1*), as suggested in new guidelines for naming movement disorders[24].

Methods

Whole-exome sequencing. Whole-exome library preparation, exon capture and sequencing were performed at the Genome Québec Innovation Center (Montréal, QC, Canada) as previously described[25]. Genomic DNA was captured using the SureSelect Human 50Mb All Exon kit v5 (Agilent Technologies, Santa Clara, CA, USA). Sequencing was performed on an Illumina HiSeq2000 (Illumina, San Diego, CA, USA) with paired-end 100-bp reads. A mean coverage of 137x was obtained and 97% of the bases were covered at more than 10x. Read alignment, variant calling, and annotation were done with a pipeline based on BWA, SAMtools, Annovar, and custom annotation scripts. All sequences were aligned to Human genome Hg19. We excluded variants with minor allele frequency greater than 5% in either the 1000 genomes project (http://browser.1000genomes.org/index.html) or the 6500 NHLBI EVS

(http://evs.gs.washington.edu/EVS), and seen in more than 30 samples from our in-house database (containing approximately 2000 samples). The WES data was further filtered to keep protein-damaging variants (nonsense, missense, frameshift, indel, and splice variants).

Antibodies and chemicals. The antibodies employed in this study were anti-XRCC1 rabbit polyclonal (Millipore; ABC738), anti-Lig3α (TL25) rabbit polyclonal[26], anti-PNKP (SK3195) rabbit polyclonal[27], rabbit Fc-fused Anti-pan-ADP-ribose binding reagent (Millipore; MABE1016), anti-poly (ADP-ribose) rabbit polyclonal (Trevigen; 4336), anti-α-tubulin rat polyclonal (Abcam; ab6160), anti-BrdU rat monoclonal, crossreacting with CldU, (BioRad; OBT0030G), anti-nucleophosmin (B23) mouse monoclonal (Invitrogen; 325200), anti-PARP1 mouse monoclonal (Serotec; MCA1522G) and anti-γH2AX mouse monoclonal (Millipore; 05-636). The secondary antibodies employed for Western blotting were HRP-conjugated goat anti-rabbit (Bio-Rad; 170-6515), goat anti-mouse (Bio-Rad; 170-6516) and rabbit anti-rat (Abcam; ab6734) and for indirect immunofluorescence were goat anti-mouse or anti-rabbit Alexa 488 (Invitrogen; A11001 and A31628), goat anti-rabbit Alexa 568 (Invitrogen; A11036), donkey anti-mouse Alexa 647 (Invitrogen; A39571) and goat anti-rat Alexa 568 (Invitrogen; A11077). Camptothecin (CPT) was purchased from Sigma and Hydrogen Peroxide (H_2O_2) was obtained from Fischer Scientific. Veliparib (ABT-888) was purchased from Selleckchem and KU0058948 hydrochloride from Axon.

Cell lines. All cell lines were tested for absence of mycoplasma. Wild type human hTERT RPE-1 cells (ATCC; CRL4000)(denoted “RPE-1” for simplicity) and their *XRCC1*$^{-/-}$ derivative (*XRCC1*$^{-/-}$ RPE-1 cells) were cultured in Dulbecco’s Modified Eagle’s Medium (DMEM/F12; Sigma) supplemented with 10% fetal calf serum and 0.01 mg/ml hygromycin B in a humidified atmosphere of 5% CO_2 at 37°C. Wild type control cells were 1BR3 (denoted 1BR in the text for simplicity) primary human fibroblasts and the lymphoblastoid cell line (LCL) 11-27 isolated from an normal unaffected control. XRCC1 patient primary fibroblasts (identifier number; 5596502b) were generated from a patient skin biopsy and the LCL cell lines HEP15-00082 and HEP15-00083 were obtained from fresh blood from,

respectively, the unaffected sibling and affected patient by EBV transformation. Appropriate patient consent was provided for preparation of primary fibroblasts. Primary human fibroblasts from a *PNKP*-mutated patient with cerebellar ataxia have been described previously[28]. Primary human fibroblasts were grown in Minimum Essential Media (MEM; Gibco) containing 15% fetal calf serum, 2 mM glutamine, and the antibiotics penicillin (100 units/ml) and streptomycin (100 µg/ml) at low oxygen (5%) at 37^{o}C. LCLs were cultured in RPMI medium (Gibco) containing 10% FBS, 2 mM glutamine and penicillin/streptomycin, in a humidified atmosphere of 5% CO_2 at 37°C.

Generation of gene edited RPE-1 cells. Guide sequences were identified using either E-CRISP (http://www.e-crisp.org/E-CRISP/) or CRISPRdirect (http://crispr.dbcls.jp). For *XRCC1* gene editing we chose the 23-mer CRISPR complementary guide RNA sequences 5'-CCGCCUCCGCCAUGUCGUGUCCU-3' & 5'-AGGGACACGACAUGGCGGAGGCGG-3' (PAM underlined) spanning *XRCC1* ORF nucleotides 12-34, and employed the 58-mer synthetic oligonucleotides (XCr2F; 5'-TTTCTTGGCTTTATATATCTTGTGGAAAGGACGAAACACCGACACGACATGGCGGAGG & XCr2R; 5'-GACTAGCCTTATTTTAACTTGCTATTTCTAGCTCTAAAACCCTCCGCCATGTCGTGTC) (Eurofins) encoding 18 bp Tru-guide[29] versions of the guide (underlined) minus the PAM. For *PARP1* gene editing we chose the 20-mer 'Tru-guide' sequences 5'-GCACCCUGACGUUGAGGUGG-3' and 5'-CCACCUCAACGUCAGGGUGC-3' (PAM underlined) spanning nucleotides 195-214 of the human *PARP1* ORF, and employed the 57-mer synthetic oligonucleotides PARP1-2F: 5'-TTTCTTGGCTTTATATATCTTGTGGAAAGGACGAAACACCGCACCCTGACGTTGAGG-3' & PARP1-2R: 5'-GACTAGCCTTATTTTAACTTGCTATTTCTAGCTCTAAAACCCTCAACGTCAGGGTGC-3' encoding the 17 bp Tru-guide versions of the guide (underlined) minus the PAM.

The relevant oligonucleotide guide pairs were annealed and extended into a 98-mer oligonucleotide duplexes using Phusion polymerase (NEB) and then subcloned into the guide RNA vector (Addgene; #41824)[30] using Gibson

Assembly (NEB). hTERT RPE-1 cells were co-transfected with the relevant guide construct/s separately (*XRCC1*$^{-/-}$, *PARP1*$^{-/-}$) or together (*XRCC1*$^{-/-}$/*PARP1*$^{-/-}$) and with the Cas9 expression construct Addgene #41815[30] using a NEON Transfection System (Invitrogen). 24 h later, the transfected cells were selected in medium containing 0.5 mg/ml G418 for 5 days and subcloned into 96-well plates. Once at sufficient cell density the subclones were analyzed for expression of the relevant protein/s by indirect immunofluorescence. Absence of the relevant protein/s in selected clones was then confirmed by Western blotting. For *XRCC1*$^{-/-}$, *PARP1*$^{-/-}$, and *XRCC1*$^{-/-}$/*PARP1*$^{-/-}$ RPE-1 cells we selected clones #3, #G7, and #D1 for further work, respectively.

Complementation of XRCC1 patient cells with recombinant XRCC1 protein. Recombinant human XRCC1 harbouring a C-terminal decahisitidine tag (denoted XRCC1-His) was expressed in E.coli from pET16b-XH and purified by metal-chelate affinity chromatography and gel filtration[3]. 1 or 2 µg of control bovine serum albumin (BSA) or purified XRCC1-His was electroporated into 1x10^5 XRCC1 patient fibroblasts using a NEON Transfection System (Invitrogen) according to the manufacturer's protocol. 18 hours later the cells were treated with CPT for 45 min, fixed, and immunostained for levels of XRCC1 and ADP-ribose as indicated.

RNA extraction, cDNA synthesis and qPCR analysis. LCLs were treated with either 100 µg/ml Cycloheximide (Sigma) or vehicle alone for 4 h and total RNA extracted with RNAeasy Kit (Qiagen) essentially as described by the manufacturer but with an additional 15 min DNAse I (Promega) digest of the samples on the column. 1 µg total RNA was annealed to oligodT(15) primer and reverse transcribed using M-MuLV RT (NEB) for 2 h at 42°C. After RNAse A digest, the cDNA was purified using PCR purification kit (Qiagen) and 1/40 of the eluate used per reaction. Three replicate qPCR reactions using ABsolute qPCR SYBR Low ROX (Thermo) were performed per experiment in a MX3005P (Agilent) thermocycler and analysed using MxPro software (Agilent). The fold change was calculated from ΔCt values relative to actin and $\Delta\Delta$Ct values relative to WT untreated for three independent experiments. Primers were:

XRCC1 exon10 forward: CAACACCCCCAAGTACAGC
XRCC1 exon 10 reverse: AGTCCAGCACCCACTCCTTAC
XRCC1 exon11 forward: TCCAGCAGTGAGGAGGATG
XRCC1 intron11 reverse: AGGCAAGAGTGGGAAGTTTG
XRCC1 exon 12 reverse: AGTGGGCTTGGTTTTGGTC
Actin forward: CTCGTCATACTCCTGCTTGC
Actin reverse: GAAGTGTGACGTGGACATCC

XRCC1 cDNA cloning. cDNA prepared as above from patient cells treated with cycloheximide was used for Phusion polymerase (NEB) amplification of full length XRCC1 transcripts using primers ATGCCGGAGATCCGCCTCCG and GGCTTGCGGCACCACCCCAT. PCR products were purified using Gel extraction kit (Qiagen), cloned using TOPO cloning kit (Thermo Fischer Scientific) and plasmids originating from single colonies purified using Miniprep kit (Qiagen) and sequenced by Sanger sequencing (Beckman Coulter).

siRNA. Wild type and patient primary fibroblasts were reverse-transfected with Lipofectamine RNA iMAX (Life Technologies) as indicated by the manufacturer, using non-targeting siRNA (ON-TARGETplus, Dharmacon) and siXRCC1 SMARTpool (Dharmacon).

Western blotting. PBS-washed cells were lysed in Laemmli buffer, heated for 10 min at 95°C, and sonicated for 30 sec using Bioruptor® Pico (Diagenode). Protein concentrations were determined using the BCA assay (Pierce). Samples were subjected to SDS PAGE, proteins transferred onto nitrocellulose membrane and detected by immunoblotting using the relevant primary and horseradish peroxidase-conjugated secondary antibodies. Peroxidase activity was detected by ECL reagent (GE Healthcare) and Amersham Hyperfilm ECL (GE Healthcare). Non-saturated film exposures were digitalized using an EPSONperfection 2400 photo scanner and quantified using ImageJ software.

Immunofluorescence and microscopy. Cells cultured on glass coverslips were fixed in 4% paraformaldehyde for 10 min at room temperature, permeabilized in methanol/acetone solution (1:1), blocked in 10% foetal calf serum and incubated

with primary antibodies for 60 min at room temperature. Following rising in PBS, coverslips were incubated with secondary antibodies at room temperature for 60 min. Finally, after washing in PBS, nuclei were counterstained with DAPI (Sigma) and coverslips mounted using anti−fading mounting reagent (Vectashield, Vector Laboratories). To measure chromatin retention of proteins, cells were pre-extracted in cold 0.2% Triton X-100 for 2 min on ice prior to fixation as above. High-resolution microscopy of fixed samples was carried out on a Zeiss AxioObserver.Z1 microscope, equipped with oil immersion objectives (Plan-Apochromat 63x/1.4 and 100x/1.4), Hamamatsu ORCA-Flash4.0 LT camera and ZEN 2 core imaging software. Automated wide-field microscopy was performed on an Olympus ScanR system (motorized IX83 microscope) with ScanR Image Acquisition and Analysis Software, 20x/0.45 (LUCPLFLN 20x PH) and 40x/0.6 (LUCPLFLN 40x PH) dry objectives and Hamamatsu ORCA-R2 digital CCD camera C10600.

ADP-ribose immunohistochemistry. Mice (P17-P23) were anaesthetized using 0.2 mg/g Euthanal (Vetoquinol UK Ltd) and perfused transcardially with PBS followed by 4% paraformaldehyde. The brains were postfixed in 4% paraformaldehyde for 48 h and stored in 25% sucrose/PBS until moulding and freezing. 7 µm sagittal sections were obtain using a cryostat (Leica CM1850). Immunohistochemistry was conducted essentially as described[4]. Briefly, slides were washed in PBS and heated until boiling in antigen retrieval buffer (Nacalai Tesque, Histo VT One). Endogenous peroxidase was blocked by incubating slides in 0.6% H_2O_2 in methanol. After incubating in blocking solution (5% goat serum, 1% BSA, 0.4% Triton-X-100 in PBS) the indicated primary antibodies were applied on overnight. The appropriate Biotin-SP-conjugated AffiniPure Goat antibody (JacksonImmuno Research, 1:500) was incubated on the slides for 1 hr followed by ABC reagent (Vectstain Elite ABC kit, Vector Laboratories) according to manufacturer's instructions. The chromogen was developed using VIP reagent (Vector VIP peroxide substrate kit, Vector laboratories, Inc.; SK-4600). Images were obtained using a Nikon Eclipse E400 mounted with Electronic Digital Eyepiece Camera CMOS (C-mount UK).

Sister chromatid exchanges. Lymphoblastoid cell lines were incubated in medium containing 8 μM chlorodeoxyuridine, 32 μM thymidine, 10 μM fluorodeoxyuridine and 200 μM cytidine (such that 20% of incorporated thymidine is replaced with chlorodeoxyuridine)[11,31] for 20 h, washed twice in media and then allowed to grow for another 20 h in medium containing 10 μM thymidine. Cells were treated with 100 ng/ml colcemid for 1 h, swollen in 75 mM KCl for 5 min at 37°C and fixed in Carnoy's fixative before preparation of metaphase spreads. Slides were allowed to air dry, rehydrated in PBS, incubated in 2 M HCl for 30 min, washed twice in 100 mM borate buffer pH 8.5 for 10 min and blocked in 10% foetal calf serum in PBS for 30 min. Further immunofluorescence and imaging was performed as above.

SSBR & DSBR assays. Alkaline comet assays were performed essentially as described[32] and inducing DNA breaks with 50 μM H_2O_2 (RPE-1 cells) or 25 μM H_2O_2 (primary fibroblasts) for 10 min on ice. For DSB repair assays, cells were irradiated with 2 Gy using Gammacell 1000 machine, and γH2AX quantified at the indicated times, afterwards.

Mouse maintenance and analysis. Animals were maintained and used under the auspices of UK Home Office project licence number 70/8300. The generation of *Parp1*$^{-/-}$ and *Xrcc1*$^{Nes\text{-}Cre}$ mice have been reported previously[4,33]. Intercrosses between *Parp1*$^{-/-}$ and *Xrcc1*$^{+/loxp}$ mice were maintained in a mixed C57/Bl6 x S129 strain and housed on a 12 h light/dark cycle with lights on at 7 am. Temperature and humidity were maintained at 21^{o}C (+/-2^{o}C) and 50% (+/-10%), respectively. All experiments were carried out under the UK Animal (Experimental Procedures) Act, 1986. Genomic DNA was extracted from biopsied tail using the REDExtract-N-Amp™ Tissue PCR Kit in accordance to the manufacturer's instructions (Sigma). For *Parp1*, the following primers were used: PARP1 F1 (5'-GTT GTG AAC GAC CTT CTG GG-3'), PARP1 R1 (5'-CCT TCC AGA AGC AGG AGA AG-3') and PARP R2 (5'-GCT TCA GTG ACA ACG TCG AG-3'). PCR products were generated by an initial denaturation step at 94°C for 2 min followed by 35 cycles of 94°C for 30 s, 54°C for 40 s and 72°C for 180 s. *Xrcc1* was amplified using the forward PC1 (5'-TAT GCT TGC TGT ACA GGG ATT GGG-3') and reverse PC2

(5'-TGG ACC ATG AAA AAG CTG TGT GC-3') primers. A 400 bp *cre* PCR product was generated using the forward Cre-3 (5'-CTG CCA CGA CCA AGT GAC AGC-3') and reverse Cre-4 (5'-ACC TGC GGT GCT AAC CAG CG-3') primers. Both *Xrcc1* and *Cre* PCR products were amplified using the following PCR conditions: initial denaturation for 5 min at 94°C followed by 35 cycles of 94°C for 30 s, 59°C for 45 s and 72°C for 45 s.

Nissl staining of paraffin-embedded sections. Brains were removed at the indicated times and placed in 10% neutral buffered formalin (3.7% formaldehyde, 3.5 g/l NaH_2PO_4, 6.5 g/l Na_2HPO_4) for 24 h and then transferred to PBS. Paraffin embedding, sagittal sectioning and Nissl staining were carried out by Propath UK Ltd (Hereford, UK) and UCL IQPath (Institute of Neurology, London, UK). Briefly, deparaffinised sectioned were stained in 0.1% cresyl violet solution (0.1% cresyl violet, 0.3% glacial acetic acid) for 3-10 minutes, rinsed in water, then 95% ethanol for 30 sto 5 min, 100% ethanol for 2 x 5 min and xylene for 2 x 5 min before mounting. Nissl-positive interneurons were counted within three randomly-selected 16875 μm^2 regions of each molecular layer, and the number of cells per μm^2 was calculated.

Rotarod analysis. To evaluate motor coordination/cerebellar ataxia, an accelerating Panlab Rotarod (Harvard Apparatus Ltd., UK) was used. The apparatus was composed of a rod with a diameter of 30 mm divided into five opaque methacrylate arnite barriers, separating the rod into five 50 mm sections. Mice were trained for three successive attempts on the day prior to assessment. For assessment, mice were positioned on the rod facing away from the experimenter whilst the rod was stationary. Once activated, the rod accelerated at 0 to 40 rpm at an acceleration rate of 5 min. Mice were rested for 15 min between each of the three trials and then positioned back on the rod for the next assessment. The time spent on the rod was recorded for each mouse and the mean time was calculated from the three independent trials.

Purkinje cell recordings. Vermis parasagittal slices (200 µm) were taken from P13-P17 mice using a vibroslicer (VT1200S, Leica Microsystems, Germany) in

ice-cold artificial cerebrospinal fluid (ACSF) containing (in mM): 125 NaCl, 2.5 KCl, 25 glucose, 1.25 NaH_2PO_4, 26 $NaHCO_3$, 1 $MgCl_2$, 2 $CaCl_2$ (bubbled with 95% O_2 and 5% CO_2, pH 7.3). Slices were maintained in ACSF at 34-35°C for 45 min and then at 23-25°C for electrophysiology. Voltage-clamp recordings of Purkinje cells were performed in cell-attached mode using a Multiclamp 700A amplifier (Molecular Devices) with pipettes (5-7 MΩ) containing 150 mM NaCl. Signals were filtered at 10 kHz and digitized at 50 kHz and analysis of spike activity performed offline using Clampfit (Molecular Devices).

Data Availability. The datasets generated during and/or analysed during the current study are available from the corresponding author on reasonable request.

Data analysis and statistics. The number of experimental repeats and statistical tests (conducted in Excel or GraphPad) are indicated in the relevant figure legends. The means of population averages from multiple independent experiments (+/-SD) are indicated. Where appropriate, power calculations were conducted using online statistical resources. Samples were not blinded but the collection and analysis of microscopic data was automated and free of user bias. No animals/samples were omitted from data points/data analyses.

Acknowledgments. We would like to thank the patient and her family for their contribution to this study. This work was selected for study by the Care4Rare Canada (Enhanced Care for Rare Genetic Diseases in Canada) Consortium Gene Discovery Steering Committee: Kym Boycott (lead; University of Ottawa), Alex MacKenzie (co-lead; University of Ottawa), Jacek Majewski (McGill University), Michael Brudno (University of Toronto), Dennis Bulman (University of Ottawa), and David Dyment (University of Ottawa). We especially thank David Dyment (University of Ottawa) for his advice and discussion. We thank Saskia vanderVelde-Visser and Janneke Schuurs-Hoeijmakers at the Radboud Nijmegen University Medical Centre for EBV transformation of the patient and sibling LCLs.

Funding. This work was funded by a MRC Programme Grant (MR/J006750/1) to KWC, a “Science without Borders” postdoctoral fellowship (CAPES Foundation, Ministry of Education, Brazil, BEX9769-13-7) to NH, and funding to GY from

Genome Canada, the Canadian Institutes of Health Research, the Ontario Genomics Institute, Ontario Research Fund, Genome Quebec, Children's Hospital of Eastern Ontario Foundation and the Hospital for Sick Children. PMcK acknowledges the NIH (NS-37956, CA-21765), the CCSG (P30 CA21765) and the American Lebanese and Syrian Associated Charities of St. Jude Children's Research Hospital for support.

1. Caldecott, K. W. Single-strand break repair and genetic disease. *Nat. Rev. Genet.* **9,** 619–631 (2008).
2. Caldecott, K. W. XRCC1 and DNA strand break repair. *DNA Repair (Amst)* **2,** 955–969 (2003).
3. Caldecott, K. W., Tucker, J. D., Stanker, L. H. & Thompson, L. H. Characterization of the XRCC1-DNA ligase III complex in vitro and its absence from mutant hamster cells. *Nucleic Acids Res* **23,** 4836–4843 (1995).
4. Lee, Y. *et al.* The genesis of cerebellar interneurons and the prevention of neural DNA damage require XRCC1. *Nat. Neurosci.* **12,** 973–980 (2009).
5. Caldecott, K. W., McKeown, C. K., Tucker, J. D., Ljungquist, S. & Thompson, L. H. An interaction between the mammalian DNA repair protein XRCC1 and DNA ligase III. *Mol Cell Biol* **14,** 68–76 (1994).
6. Tebbs, R. S. *et al.* Requirement for the Xrcc1 DNA base excision repair gene during early mouse development. *Dev. Biol.* **208,** 513–529 (1999).
7. Tebbs, R. S., Thompson, L. H. & Cleaver, J. E. Rescue of Xrcc1 knockout mouse embryo lethality by transgene-complementation. *DNA Repair (Amst)* **2,** 1405–1417 (2003).
8. Bradley, M. O. & Kohn, K. W. X-ray induced DNA double strand break production and repair in mammalian cells as measured by neutral filter elution. *Nucleic Acids Res* **7,** 793–804 (1979).
9. Thompson, L. H. & West, M. G. XRCC1 keeps DNA from getting stranded. *Mutat Res* **459,** 1–18 (2000).
10. Thompson, L. H. *et al.* A CHO-cell strain having hypersensitivity to mutagens, a defect in DNA strand-break repair, and an extraordinary baseline frequency of sister-chromatid exchange. *Mutat Res* **95,** 427–440 (1982).
11. Dillehay, L. E., Thompson, L. H., Minkler, J. L. & Carrano, A. V. The relationship between sister-chromatid exchange and perturbations in DNA replication in mutant EM9 and normal CHO cells. *Mutat Res* **109,** 283–296 (1983).
12. Takashima, H. *et al.* Mutation of TDP1, encoding a topoisomerase I-dependent DNA damage repair enzyme, in spinocerebellar ataxia with axonal neuropathy. *Nat Genet* **32,** 267–272 (2002).
13. El-Khamisy, S. F. *et al.* Defective DNA single-strand break repair in spinocerebellar ataxia with axonal neuropathy-1. *Nature* **434,** 108–113 (2005).
14. Moreira, M. C. *et al.* The gene mutated in ataxia-ocular apraxia 1 encodes the new HIT/Zn-finger protein aprataxin. *Nat Genet* **29,** 189–193 (2001).
15. Bras, J. *et al.* Mutations in PNKP cause recessive ataxia with oculomotor

apraxia type 4. *Am J Hum Genet* **96,** 474–479 (2015).
16. Shen, J. *et al.* Mutations in PNKP cause microcephaly, seizures and defects in DNA repair. *Nat Genet* **42,** 245–249 (2010).
17. Eliasson, M. J. *et al.* Poly(ADP-ribose) polymerase gene disruption renders mice resistant to cerebral ischemia. *Nat. Med.* **3,** 1089–1095 (1997).
18. Chiarugi, A. Poly(ADP-ribose) polymerase: killer or conspirator? The 'suicide hypothesis' revisited. *Trends Pharmacol. Sci.* **23,** 122–129 (2002).
19. Katyal, S. *et al.* Aberrant topoisomerase-1 DNA lesions are pathogenic in neurodegenerative genome instability syndromes. *Nat. Neurosci.* (2014). doi:10.1038/nn.3715
20. Hou, Y., Song, H., Croteau, D. L., Akbari, M. & Bohr, V. A. Genome instability in Alzheimer disease. *Mech. Ageing Dev.* (2016). doi:10.1016/j.mad.2016.04.005
21. Shiwaku, H. & Okazawa, H. Impaired DNA damage repair as a common feature of neurodegenerative diseases and psychiatric disorders. *Curr. Mol. Med.* **15,** 119–128 (2015).
22. Narciso, L. *et al.* The Response to Oxidative DNA Damage in Neurons: Mechanisms and Disease. *Neural Plast.* **2016,** 3619274 (2016).
23. Murai, J. *et al.* Trapping of PARP1 and PARP2 by Clinical PARP Inhibitors. *Cancer Res* **72,** 5588–5599 (2012).
24. Marras, C. *et al.* Nomenclature of genetic movement disorders: Recommendations of the international Parkinson and movement disorder society task force. *Mov. Disord.* **31,** 436–457 (2016).
25. Tetreault, M. *et al.* Whole-exome sequencing identifies novel ECHS1 mutations in Leigh syndrome. *Hum. Genet.* **134,** 981–991 (2015).
26. Cappelli, E. *et al.* Involvement of XRCC1 and DNA ligase III gene products in DNA base excision repair. *J Biol Chem* **272,** 23970–23975 (1997).
27. Breslin, C. & Caldecott, K. W. DNA 3'-phosphatase activity is critical for rapid global rates of single-strand break repair following oxidative stress. *Mol Cell Biol* **29,** 4653–4662 (2009).
28. Poulton, C. *et al.* Progressive cerebellar atrophy and polyneuropathy: expanding the spectrum of PNKP mutations. *Neurogenetics* (2012). doi:10.1007/s10048-012-0351-8
29. Fu, Y., Sander, J. D., Reyon, D., Cascio, V. M. & Joung, J. K. Improving CRISPR-Cas nuclease specificity using truncated guide RNAs. *Nat. Biotechnol.* **32,** 279–284 (2014).
30. Mali, P. *et al.* RNA-guided human genome engineering via Cas9. *Science* **339,** 823–826 (2013).
31. Pinkel, D., Thompson, L. H., Gray, J. W. & Vanderlaan, M. Measurement of sister chromatid exchanges at very low bromodeoxyuridine substitution levels using a monoclonal antibody in Chinese hamster ovary cells. *Cancer Res* **45,** 5795–5798 (1985).
32. Breslin, C. *et al.* Measurement of chromosomal DNA single-strand breaks and replication fork progression rates. *Meth. Enzymol.* **409,** 410–425 (2006).
33. Wang, Z. Q. *et al.* Mice lacking ADPRT and poly(ADP-ribosyl)ation develop normally but are susceptible to skin disease. *Genes Dev* **9,** 509–520 (1995).

a

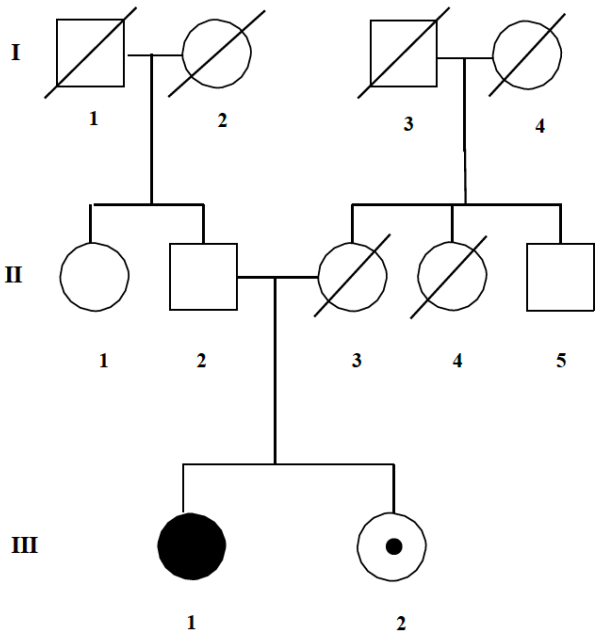

b

Age/sex	47/F
Onset (yr)	28
Presenting Symptom	Gait ataxia
Intelligence	Normal
Muscle weakness	Mild (Distal Muscles)
Dystonia	No
Sensory Disturbance:	
Touch and Pain	Normal
Vibration	Decreased
Position Sense	Decreased
Ataxia:	
Gait	Yes (Severe)
Dysmetria	Yes
Dysarthria	Yes
Dysdiadochokinesia	Yes
Deep Tendon Reflex	Absent
Oculomotor Apraxia	Yes
MRI	Cerebellar Atrophy
Motor Nerve Conduction Velocity:	
upper limbs	Mild reduction/Normal
lower limbs	Mild reduction/Normal
Sensory Nerve Conduction Velocity:	
upper limbs	Absent/not recordable
lower limbs	Absent/not recordable

c

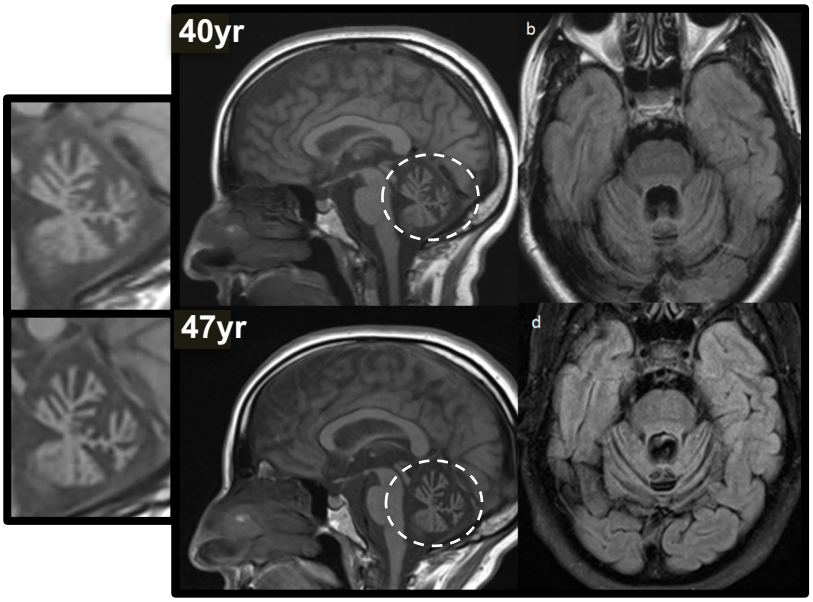

d

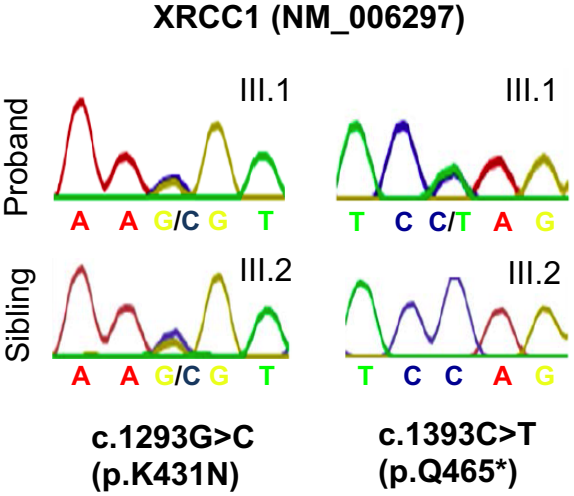

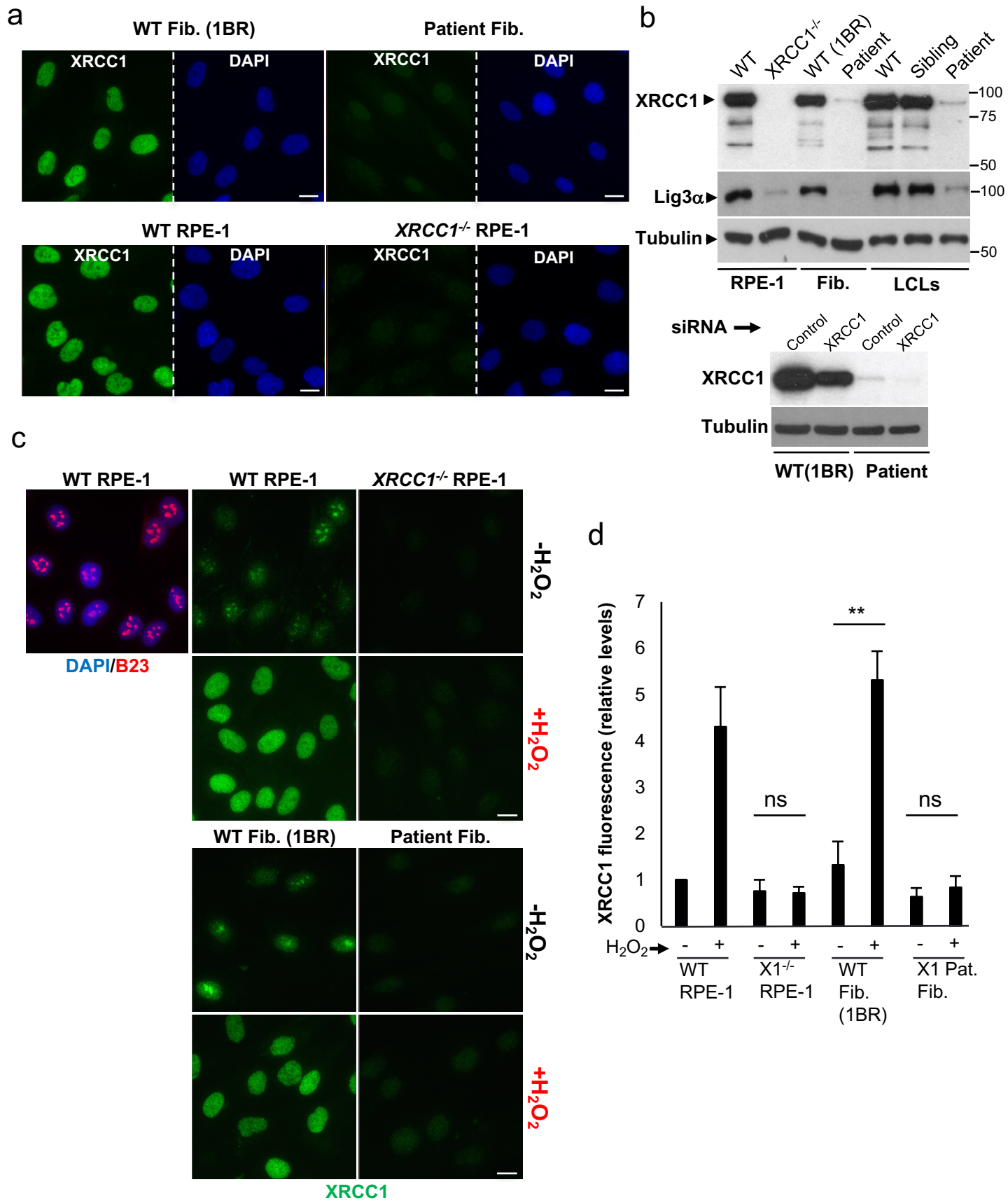
a
WT Fib. (1BR)
Patient Fib.
XRCC1
DAPI
WT RPE-1
XRCC1-/- RPE-1
b
WT
XRCC1-/-
WT (1BR)
Patient
WT
Sibling
Patient
XRCC1
Lig3α
Tubulin
100
75
50
100
50
RPE-1
Fib.
LCLs
siRNA
Control
XRCC1
Control
XRCC1
XRCC1
Tubulin
WT(1BR)
Patient
c
WT RPE-1
WT RPE-1
XRCC1-/- RPE-1
-H2O2
+H2O2
DAPI/B23
WT Fib. (1BR)
Patient Fib.
-H2O2
+H2O2
XRCC1
d
XRCC1 fluorescence (relative levels)
0
1
2
3
4
5
6
7
**
ns
ns
H2O2
-
+
-
+
-
+
-
+
WT RPE-1
X1-/- RPE-1
WT Fib. (1BR)
X1 Pat. Fib.

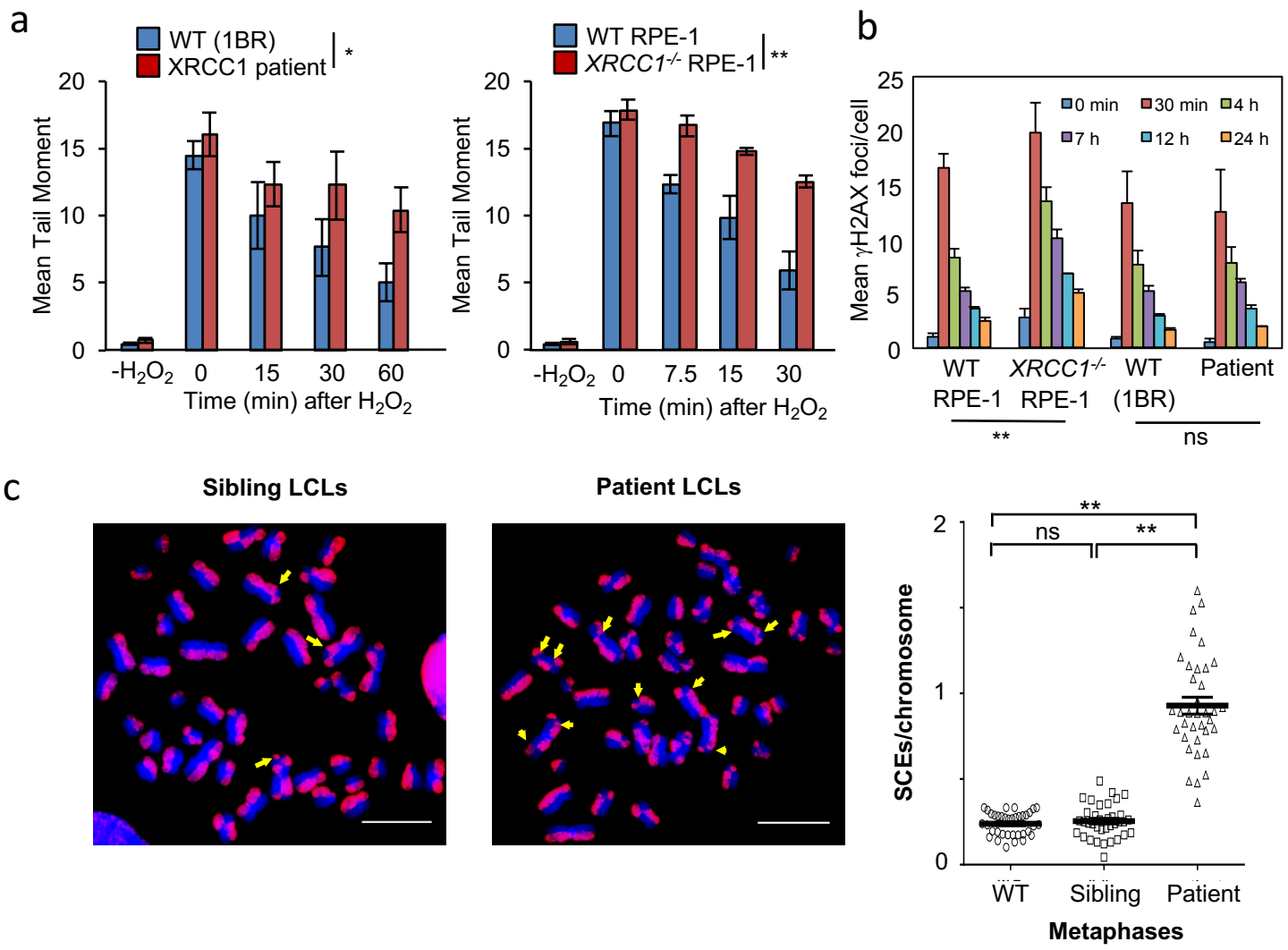
a
WT (1BR)
XRCC1 patient
*
Mean Tail Moment
20
15
10
5
0
-H2O2
0
15
30
60
Time (min) after H2O2
WT RPE-1
XRCC1-/- RPE-1
**
Mean Tail Moment
20
15
10
5
0
-H2O2
0
7.5
15
30
Time (min) after H2O2
b
Mean γH2AX foci/cell
25
20
15
10
5
0
0 min
30 min
4 h
7 h
12 h
24 h
WT RPE-1
XRCC1-/- RPE-1
WT (1BR)
Patient
**
ns
c
Sibling LCLs
Patient LCLs
SCEs/chromosome
2
1
0
**
ns
**
WT
Sibling
Patient
Metaphases

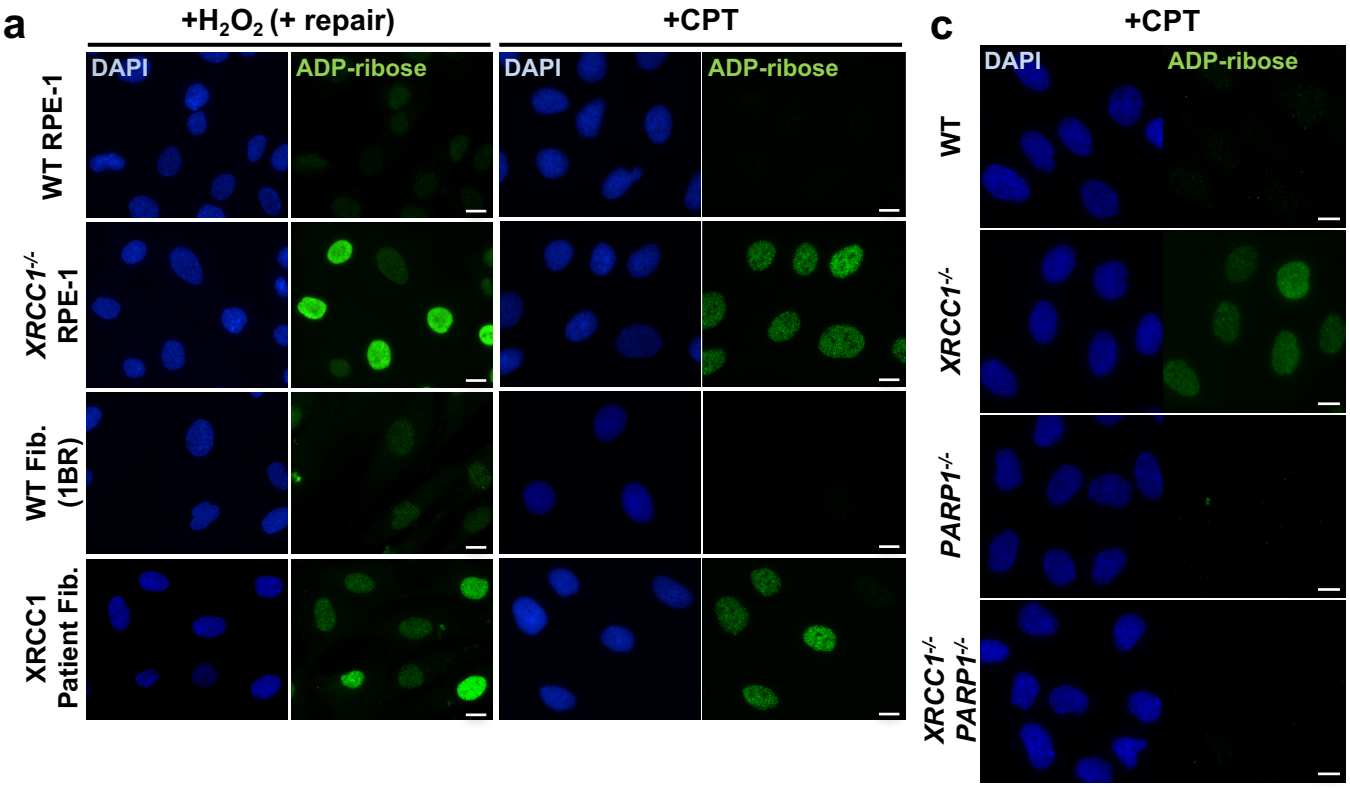
a
+H2O2 (+ repair)
+CPT
DAPI
ADP-ribose
WT RPE-1
XRCC1-/- RPE-1
WT Fib. (1BR)
XRCC1 Patient Fib.
c
+CPT
WT
XRCC1-/-
PARP1-/-
XRCC1-/- PARP1-/-

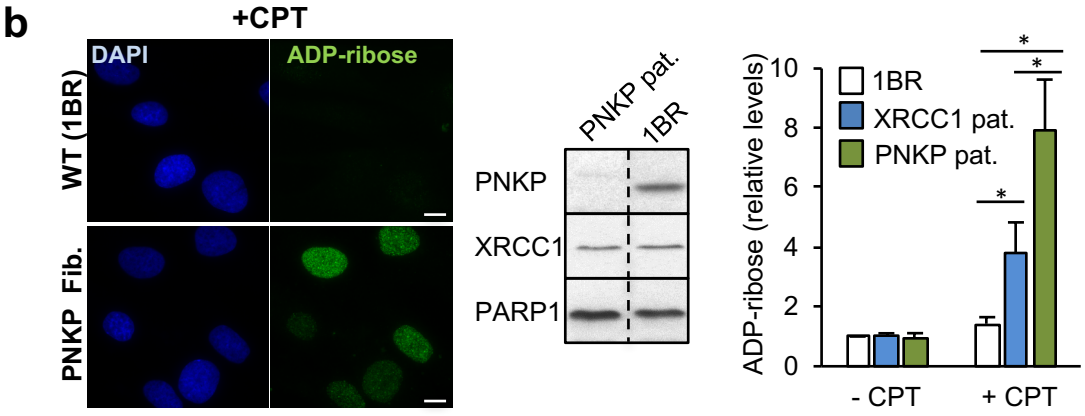
b
+CPT
WT (1BR)
PNKP Fib.
PNKP pat.
1BR
PNKP
XRCC1
PARP1
ADP-ribose (relative levels)
1BR
XRCC1 pat.
PNKP pat.
- CPT
+ CPT

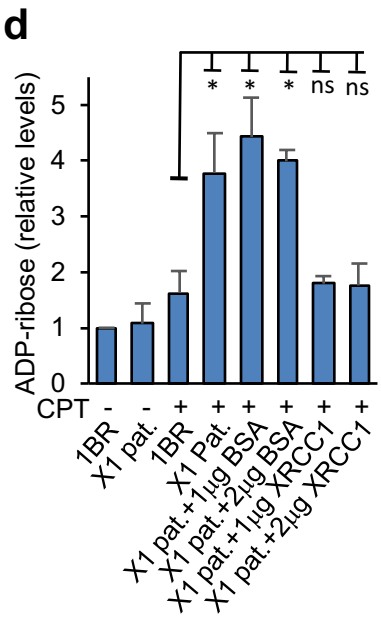
d
ADP-ribose (relative levels)
CPT
1BR
X1 pat.
1BR
X1 Pat.
X1 pat.+1µg BSA
X1 pat.+2µg BSA
X1 pat.+1µg XRCC1
X1 pat.+2µg XRCC1
ns

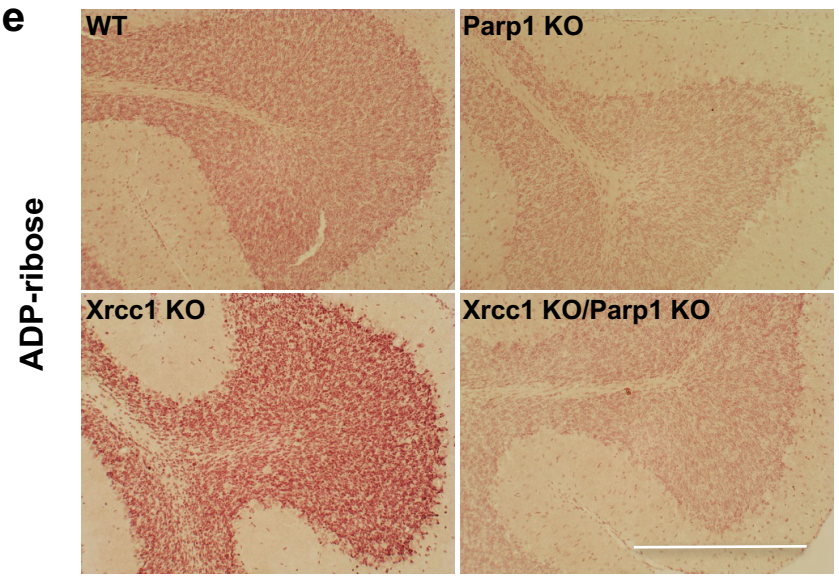
e
ADP-ribose
WT
Parp1 KO
Xrcc1 KO
Xrcc1 KO/Parp1 KO

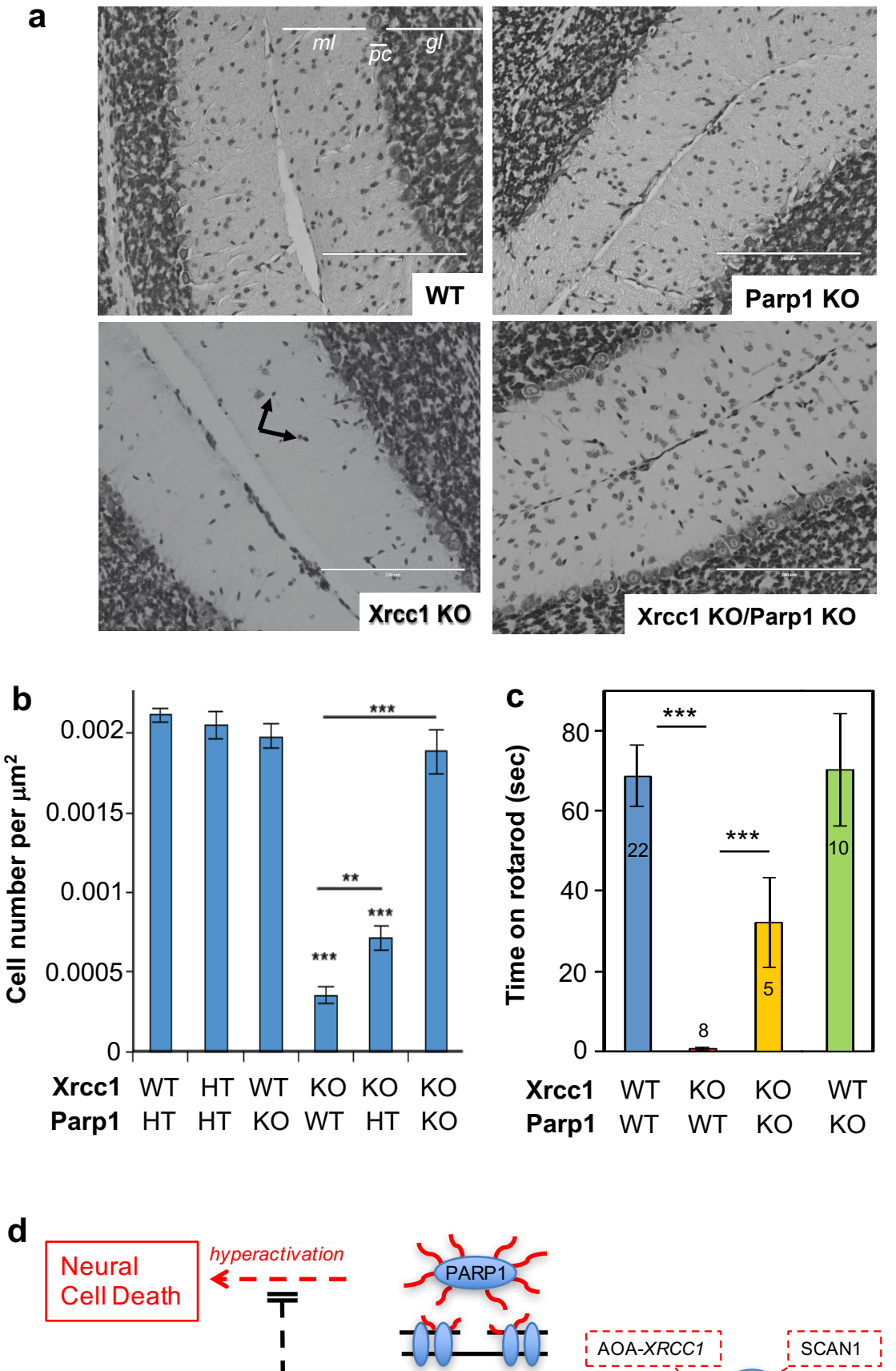
a
ml
pc
gl
WT
Parp1 KO
Xrcc1 KO
Xrcc1 KO/Parp1 KO
b
Cell number per µm²
0.002
0.0015
0.001
0.0005
0
***
**
***
***
Xrcc1 WT HT WT KO KO KO
Parp1 HT HT KO WT HT KO
c
Time on rotarod (sec)
80
60
40
20
0
***
***
22
8
5
10
Xrcc1 WT KO KO WT
Parp1 WT WT KO KO
d
Neural Cell Death
hyperactivation
PARP1
SSB repair
AOA-XRCC1
SCAN1
TDP1
Polβ
Lig3
XRCC1
APTX
PNKP
AOA1
AOA4/MCSZ